Journal of Materials Chemistry A

ROYAL SOCIETY OF CHEMISTRY

PAPER

View Article Online
View Journal | View Issue

Check for updates

Cite this: J. Mater. Chem. A, 2023, 11, 1810

Realizing 18.03% efficiency and good junction characteristics in organic solar cells *via* hydrogen-bonding interaction between glucose and ZnO electron transport layers†

Zhongqiang Wang, *[a] Yabing Ren,[a] Jiawei Meng,[a] Xuefeng Zou,[a] Shenjian Wang,[a] Min Zhao,[a] Hua Wang,[a] Yuying Hao,[a] Bingshe Xu,[a] Ergang Wang *[b] and Shougen Yin *[c]

Received 8th October 2022
Accepted 19th December 2022

DOI: 10.1039/d2ta07856b

rsc.li/materials-a

Electron transport layers (ETLs) with excellent electron extraction capability are essential for realizing high efficiency in organic solar cells (OSCs). A sol–gel-processed ZnO ETL is widely used in OSCs due to its high mobility and suitable work function. However, the existence of defects usually results in low photovoltaic performance during the operation of OSCs. In this work, glucose (Gl) was used to passivate free OH traps *via* hydrogen-bonding interaction and formed ZnO/Gl ETLs with ZnO, which exhibited improved electron extraction capability and reduced trap defect density. Thus, a champion efficiency of 18.03% was obtained in a PM6:Y6 light absorber-based cell, which is >11% higher than that of the reference cell (16.15%) with a pristine ZnO ETL. Impressive enhancements by >11% were also observed in different fullerene and non-fullerene light absorber-based cells relative to that of the reference cell. This study demonstrates a new strategy to design ETLs for realizing high efficiency in OSCs.

Open Access Article. Published on 19 December 2022. Downloaded on 2/7/2026 11:24:43 AM.
This article is licensed under a Creative Commons Attribution 3.0 Unported Licence.

1. Introduction

Organic solar cells (OSCs) have attracted great attention due to their advantages such as mechanical flexibility, light weight, and solution processing over their inorganic counterparts.[1–4] Recently, the power conversion efficiency (PCE) of OSCs has surpassed 19% in single-junction cells.[5–9] The significant progress in OSCs can be attributed to the development of organic semiconductors covering a wide range of the solar spectrum, the optimization of device structures and deep understanding of device physics.[10–13] To realize efficient light-to-electron conversion, hole transport layers (HTLs) and electron transport layers (ETLs) that can facilitate charge extraction and transport play important roles, apart from the light absorbers responsible for exciton generation and dissociation, and charge transport.[14] Hence, the development of suitable HTLs and ETLs is critical to achieving good junction characteristics and high efficiency in OSCs.

Compared to the conventional OSC device structure of glass/ITO/PEDOT:PSS/light absorbers/ETL/Al, an inverted structure, *i.e.*, glass/ITO/ETL/light absorbers/HTL/Al, possesses reverse junction polarity, which usually shows higher PCE and better lifetime in OSCs. To construct efficient OSCs with an inverted structure, excellent ETLs such as ZnO, SnO_2, TiO_x, and CsO_x exhibit good transparence, high electron mobility and suitable work function (WF).[15–18] ZnO is widely used as an ETL material due to its excellent optical and electrical properties, good film-forming properties, and low annealing temperature.[19–21] The sol–gel technique is a simple and effective method that is used to deposit ZnO ETLs. However, sol–gel-processed ZnO ETLs show surface and inside defects, such as Zn interstitials, free hydroxide (–OH), and oxygen vacancies, which lead to inferior electrical properties.[22–24] These defects in ZnO ETLs act as trap centers in OSCs, resulting in low photovoltaic performance and inferior junction characteristics. Hence, it is essential to develop an efficient passivation strategy to reduce defects for achieving good charge extraction characteristics and high efficiency in OSCs with sol–gel-processed ZnO ETLs.

[a]*Key Laboratory of Interface Science and Engineering in Advanced Materials, Ministry of Education, Research Center of Advanced Materials Science and Technology, Taiyuan University of Technology, Taiyuan, 030024, China. E-mail: wangzhongqiang@tyut.edu.cn*

[b]*Department of Chemistry and Chemical Engineering, Chalmers University of Technology, Göteborg, SE-412 96, Sweden. E-mail: ergang@chalmers.se*

[c]*Key Laboratory of Display Materials and Photoelectric Devices (Ministry of Education), School of Materials Science and Engineering, Tianjin University of Technology, Tianjin 300384, China. E-mail: sgyin@tjut.edu.cn*

† Electronic supplementary information (ESI) available: Experimental section; device architecture of OSCs; chemical structures of PTB7-Th, $PC_{71}BM$, PM6, Y6, and glucose; XPS spectra of Gl and ZnO/Gl; *J–V* characteristics of cells using different ETLs; $\log J_{ph}$ *versus* $\log V_{eff}$ of cells using different ETLs; $P(E,T)$ *versus* $\log V_{eff}$ of cells using different ETLs; $P(E,T)$ obtained from cells with different ETLs; $\log J_{sc}$ *versus* $\log P_{light}$ of OSCs with ZnO and ZnO/Gl(*X*) ETLs; V_{oc} *versus* $\log P_{light}$ of OSCs with ZnO and ZnO/Gl(*X*) ETLs; photovoltaic parameters extracted from *J–V* curves. See DOI: https://doi.org/10.1039/d2ta07856b

This journal is © The Royal Society of Chemistry 2023

Open Access Article. Published on 19 December 2022. Downloaded on 2/7/2026 11:24:43 AM.
This article is licensed under a Creative Commons Attribution 3.0 Unported Licence.

In this contribution, we demonstrate an excellent ETL which was processed by depositing glucose (Gl) on top of sol–gel-processed ZnO films. Our study proved that the deposition of Gl could passivate surface defects of free OH groups due to the hydrogen bond interaction between ZnO and Gl. Thus, good junction properties and high efficiency were achieved from ZnO/Gl ETL-based OSCs. A low-cost and facile strategy was developed to form highly efficient ETLs for OSCs.

2. Results and discussion

X-ray photoelectron spectroscopy (XPS) was used to unravel the interaction between ZnO and Gl films. The XPS spectra of ZnO and ZnO/Gl are shown in Fig. 1a and ESI Fig. S2.† The binding energy peak at 288.88 eV corresponds to the C=O group. This peak shifted to 288.58 eV after the deposition of Gl, which signifies interaction between ZnO and Gl.

The FTIR spectra of Gl and ZnO/Gl are shown in Fig. 1b. According to the literature, the absorption peak at around 1249 cm^{-1} from the pristine Gl sample is due to OH vibration.[25] This peak was shifted to 1241 cm^{-1} after the deposition of Gl on the ZnO film, which indicated that the O–H vibration was influenced by the formation of a hydrogen bond between CO in Gl and the free OH on the surface of ZnO. The CO and OH groups form hydrogen bonds because of the electron transfer from CO to OH.[26] The trap sites caused by free OH in sol–gel ZnO could obviously be reduced by hydrogen-bonding interactions between CO and OH groups. The trap passivation should have improved the electron extraction and transport properties of the ZnO ETL. It was expected that free OH passivation of ZnO could lead to impressive photovoltaic performance in Gl-passivated ZnO ETL-based cells.

The thickness of ZnO ETLs was fixed to be 40 nm based on our previous work.[27] The Gl-modified ZnO ETLs were named ZnO/Gl(X) (X stands for the spin speed). To obtain the optimal photovoltaic performance, the thicknesses of Gl were tuned by varying the spin speed from 2000 to 5000 rpm under a Gl concentration of 2 mg mL^{-1}. The current density–voltage (J–V) curves and external quantum efficiency (EQE) spectra are shown in Fig. 2a, b and S3.† As displayed in Fig. 2a, a PCE of 16.15% with an open circuit voltage (V_{oc}) of 0.834 V, a short circuit current density (J_{sc}) of 25.84 mA cm^{-2}, and a fill factor (FF) of 74.72% was obtained from the PM6:Y6 light absorber-based cell with a pristine ZnO ETL, which is in good agreement with reported values.[24] It is clear that the cells showed higher PCE when the spin speeds were over 4000 rpm compared to the reference cell. Due to the insulation of Gl, decreased PCEs were recorded when the Gl spin speed was lower than 4000 rpm, as shown in Fig. 2c. The highest PCE of 18.03%, with a V_{oc} of 0.826 V, a J_{sc} of 28.65 mA cm^{-2}, and a FF of 76.20%, was achieved from cells with the ZnO/Gl(4000) ETL, which is an improvement by 11% relative to that of the reference cell with a ZnO ETL due to the increase in J_{sc} and FF, as summarized in Table 1. The reported PCEs based on the PM6:Y6 blend are summarized in Fig. 2d. To the best of our knowledge, the PCE achieved in this work is one of the highest values recorded from PM6:Y6 binary light absorber-based OSCs.

As displayed in Fig. 2b, the cell with the ZnO/Gl(4000) ETL showed the highest photo-response especially in the near-infrared region, which resulted in improved J_{cal}. The enhancement in EQE spectra was in line with the variation of J_{sc} extracted from J–V curves, which proved the enhancement in the performances of cells with ZnO/Gl(X) ETLs.

The morphology of ETLs has a significant impact on the interfacial contact and charge transfer in OSCs.[28] Atomic force microscopy (AFM) was used to investigate the morphology variation of the ZnO ETL before and after Gl deposition. The two-dimensional (2-D) and the corresponding three-dimensional (3-D) AFM images are displayed in Fig. 3. As depicted in Fig. 3a and b, root-mean-square (RMS) roughness values of 0.512 and 0.318 nm were obtained from the pristine and Gl-modified ZnO films, respectively. The smooth surface of ZnO/Gl(X) ETLs would be of great benefit to the photovoltaic performance and junction characteristics of the OSCs.

Good junction characteristics are necessary for achieving high photovoltaic performance in OSCs. To evaluate the junction properties, the ideal diode equation was used to analyze the J–V characteristics of cells with ZnO and ZnO/Gl(X) ETLs without illumination, which is expressed as:

$$-J = J_{ph} - J_0\left\{\exp\left[\frac{q(V - JR_s)}{nKT}\right] - 1\right\} - \frac{V - JR_s}{R_{sh}} \quad (1)$$

where J, J_{ph}, J_0, and V are the current density, photocurrent density, saturation current density and applied bias,

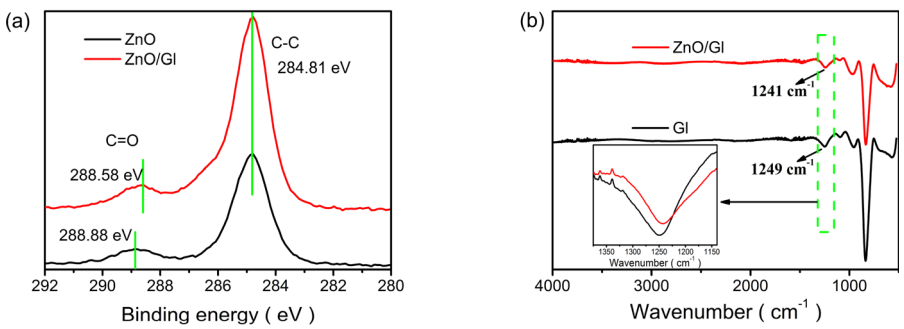

Fig. 1 (a) XPS spectra of ZnO and ZnO/Gl films and (b) FTIR spectra of Gl and ZnO/Gl films (the inset shows enlarged FTIR absorption bands in the range 1375–1140 cm^{-1}).

Open Access Article. Published on 19 December 2022. Downloaded on 2/7/2026 11:24:43 AM.
This article is licensed under a Creative Commons Attribution 3.0 Unported Licence.

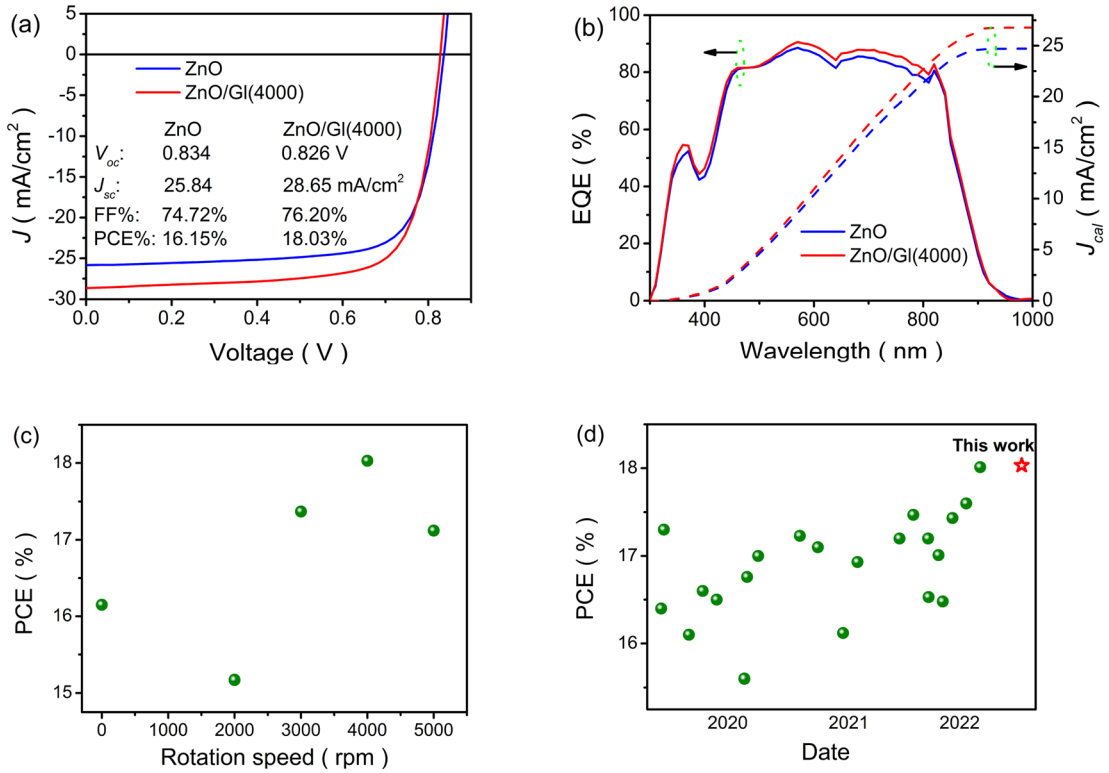

Fig. 2 (a) J–V curves of cells based on a PM6:Y6 light absorber using ZnO and ZnO/Gl(4000) as ETLs, (b) external quantum efficiency (EQE) and integrated current density (J_{cal}) of cells using ZnO and ZnO/Gl(4000) as ETLs, (c) the highest PCE obtained in cells with different ETLs, and (d) the reported PCE in binary PM6:Y6-based cells.

Table 1 Photovoltaic parameters of cells with ZnO and ZnO/Gl(X) ETLs spin-coated with a rotation speed from 2000 to 5000 rpm[a]

ETLs	V_{oc} (V)	J_{sc} (mA cm^{-2})	FF (%)	PCE (%)
ZnO	0.833 ± 0.003	24.59 ± 1.25	73.41 ± 1.31	16.00 ± 0.15
	0.834	25.84	74.72	16.15
ZnO/Gl(2000)	0.817 ± 0.003	25.53 ± 1.33	67.37 ± 1.50	14.93 ± 0.24
	0.820	26.86	68.87	15.17
ZnO/Gl(3000)	0.824 ± 0.003	27.11 ± 1.28	72.56 ± 1.46	17.16 ± 0.21
	0.827	28.39	74.02	17.37
ZnO/Gl(4000)	0.824 ± 0.003	27.35 ± 1.30	74.75 ± 1.45	17.83 ± 0.20
	0.826	28.65	76.20	18.03
ZnO/Gl(5000)	0.823 ± 0.003	26.37 ± 1.29	73.60 ± 1.30	17.01 ± 0.11
	0.826	27.66	74.90	17.12

[a] The light absorber is a non-fullerene blend of PM6:Y6.

respectively, while R_s and R_{sh} represent the series and shunt resistances, n is the ideality factor, K is the Boltzmann constant, T is the absolute temperature, and q is the elementary charge.

Without illumination ($J_{ph} = 0$), eqn (1) can be simplified as:

$$-J = -J_0\left\{\exp\left[\frac{q(V - JR_s)}{nKT}\right] - 1\right\} - \frac{V - JR_s}{R_{sh}} \quad (2)$$

The parameters of n, J_0, R_{sh}, and R_s can be evaluated by fitting J–V curves with eqn (2). The dark state J–V curves obtained from cells with ZnO and ZnO/Gl(4000) ETLs are plotted in Fig. 4. The evaluated parameters are also summarized in Fig. 4. It has been proved that n is highly related to the interfaces of solar cells. A decreased n of 1.62 was obtained from a ZnO/Gl(4000) ETL-based cell, whereas n was found to be 2.01 for the cell with the ZnO ETL, which indicated better junction properties in this cell.

J_0 is part of the reverse current density in diodes, which is independent of reverse bias. A low J_0 means that ZnO ETLs possess excellent hole blocking capability.[29] In comparison with the reference cell with a J_0 of 3×10^{-10} A cm^{-2}, the cell with ZnO/Gl(4000) as the ETL showed a lower J_0 of 1×10^{-10} A cm^{-2}, as depicted in Fig. 4. The decreased J_0 value indicated superior hole blocking capability of Gl-modified ZnO, which further

 This journal is © The Royal Society of Chemistry 2023

Open Access Article. Published on 19 December 2022. Downloaded on 2/7/2026 11:24:43 AM.
This article is licensed under a Creative Commons Attribution 3.0 Unported Licence.

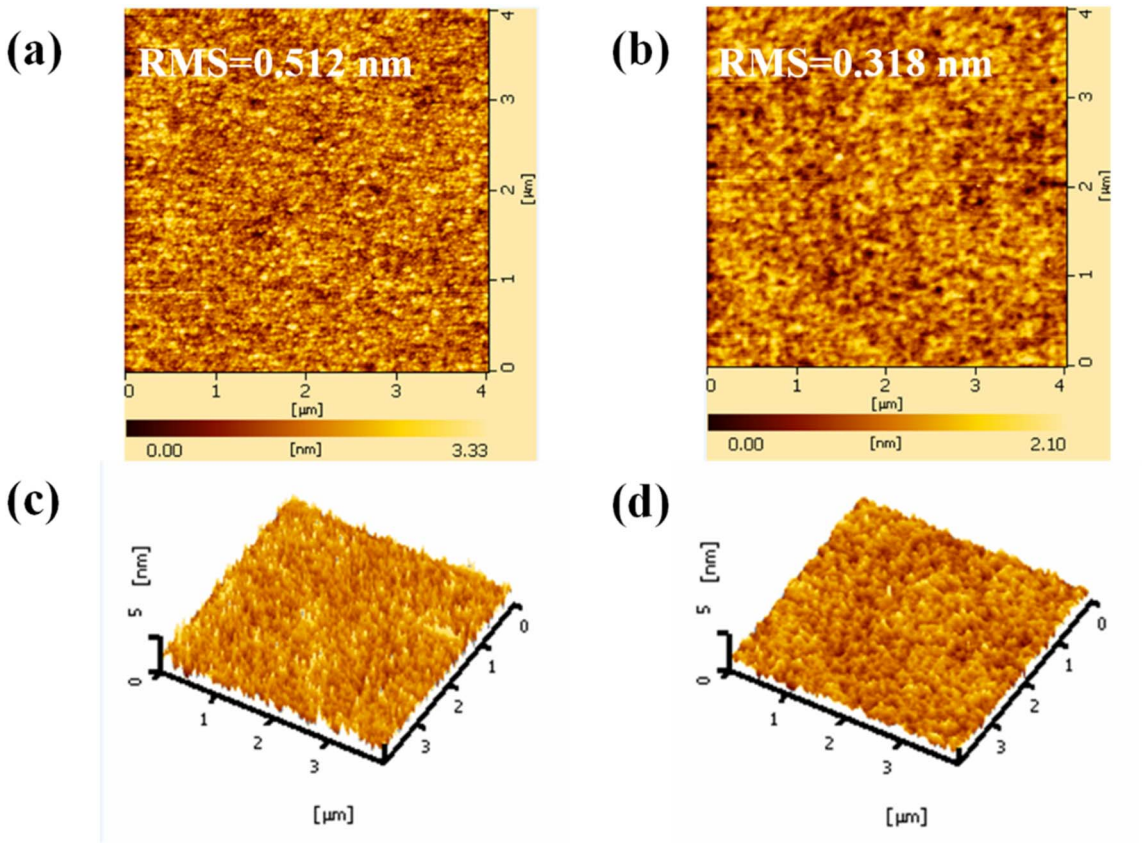

Fig. 3 Two-dimensional (2-D) AFM images (4.0 × 4.0 μm^2) of ZnO (a) and ZnO/Gl(4000) ETLs (b), and 3-D AFM images (4.0 × 4.0 μm^2) of ZnO (c) and ZnO/Gl(4000) ETLs (d).

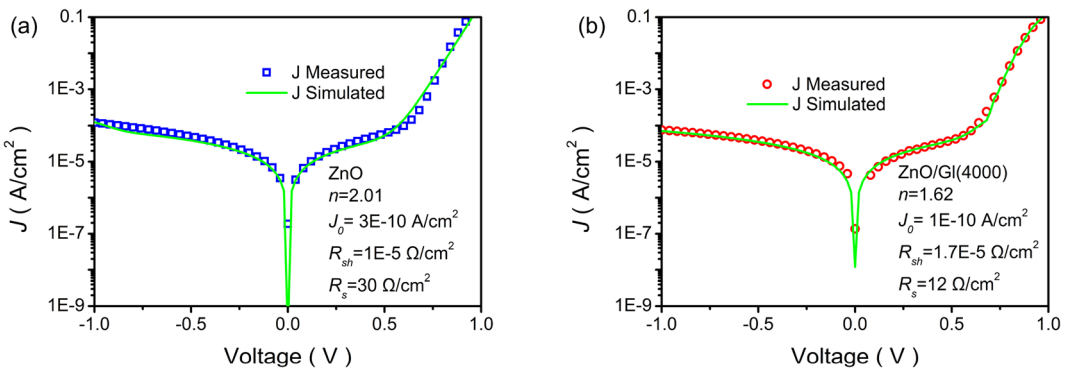

Fig. 4 Measured (blue squares or red circles) and simulated (green solid lines) *J*–*V* curves without illumination: (a) cell with the pristine ZnO ETL and (b) cell with the ZnO/Gl(4000) ETL.

confirmed the good junction characteristics in these cells. The superior hole blocking capability contributed to the improved FF in OSCs.

To understand the defect-assisted recombination process, electron-only devices with different ETLs were made to analyze the voltage of the trap-filled limit (V_{TFL}). As shown in Fig. 5a, three different regions are observed in the double-log *J*–*V* curves of electron-only devices. In the TFL region, all traps are filled with the injected carriers, which could reflect the defect passivation of ZnO ETLs. A reduced V_{TFL} of 0.63 V was obtained from the cell with the ZnO/Gl(4000) ETL, suggesting that the introduction of Gl reduced the defect density of ZnO. The suppressed trap-assisted recombination was beneficial to realizing efficient electron extraction and transport in ZnO/Gl(*X*) ETL-based cells, resulting in improved J_{sc} and FF.

To further study the influence of Gl, electrical impedance spectroscopy (EIS) was utilized to compare the electrical characteristics of cells with different ETLs,[30] as plotted in Fig. 5b.

Open Access Article. Published on 19 December 2022. Downloaded on 2/7/2026 11:24:43 AM.
This article is licensed under a Creative Commons Attribution 3.0 Unported Licence.

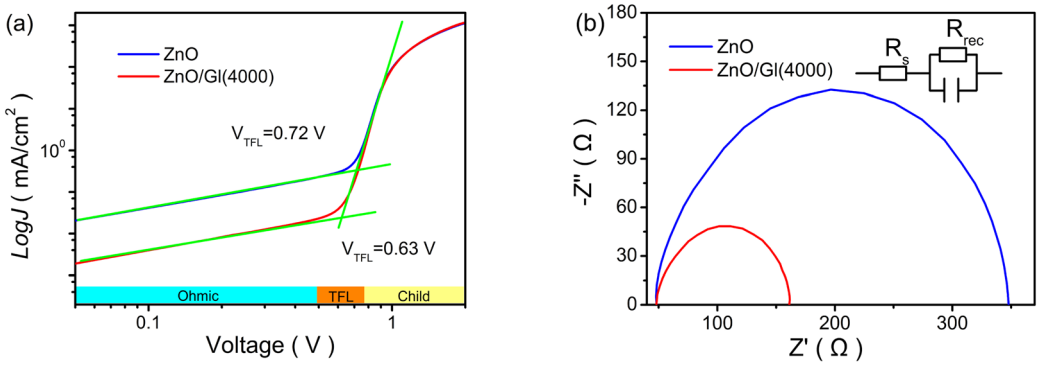

Fig. 5 (a) Electron-only devices with pristine ZnO and ZnO/Gl(4000) ETLs and (b) EIS spectra of cells with pristine ZnO and ZnO/Gl(4000) ETLs (the inset represents the equivalent circuit).

The transport resistance was extracted from the EIS spectra by fitting with the equivalent circuit. It was clear that the cell with the ZnO/Gl(4000) ETL exhibited a shorter diameter compared to that of the cell with the pristine ZnO ETL. The short diameter meant low transport resistance, which also contributed to the enhanced photovoltaic performance in cells with ZnO/Gl(X) ETLs.

The electron extraction capability of ETLs is directly affected by the charge transport and extraction processes in OSCs, which can be analyzed by the exciton decay dynamics of time-resolved photoluminescence (TRPL) spectra,[31] as shown in Fig. 6a. The extracted lifetimes from the samples of ZnO/PM6 and ZnO/Gl(4000)/PM6 were 2.41 and 1.47 ns, respectively. The decreased lifetime meant better electron extraction capability of the ZnO/Gl(4000) ETL compared to the ZnO ETL, resulting in efficient charge extraction and transport processes in ZnO/Gl(X) ETL-based cells.

Moreover, photocurrent densities (J_{ph}) under different effective voltages (V_{eff}) of cells were compared to reveal the exciton generation behavior.[32,33] Fig. 6b and S4† show the plots of log J_{ph} *versus* log V_{eff}. The maximum exciton generation rate (G_{max}) of cells was calculated from the plots of log J_{ph}–log V_{eff}, as summarized in Fig. 6c. A clear enhancement in G_{max} was observed in cells with ZnO/Gl(X) ETLs. This result indicates

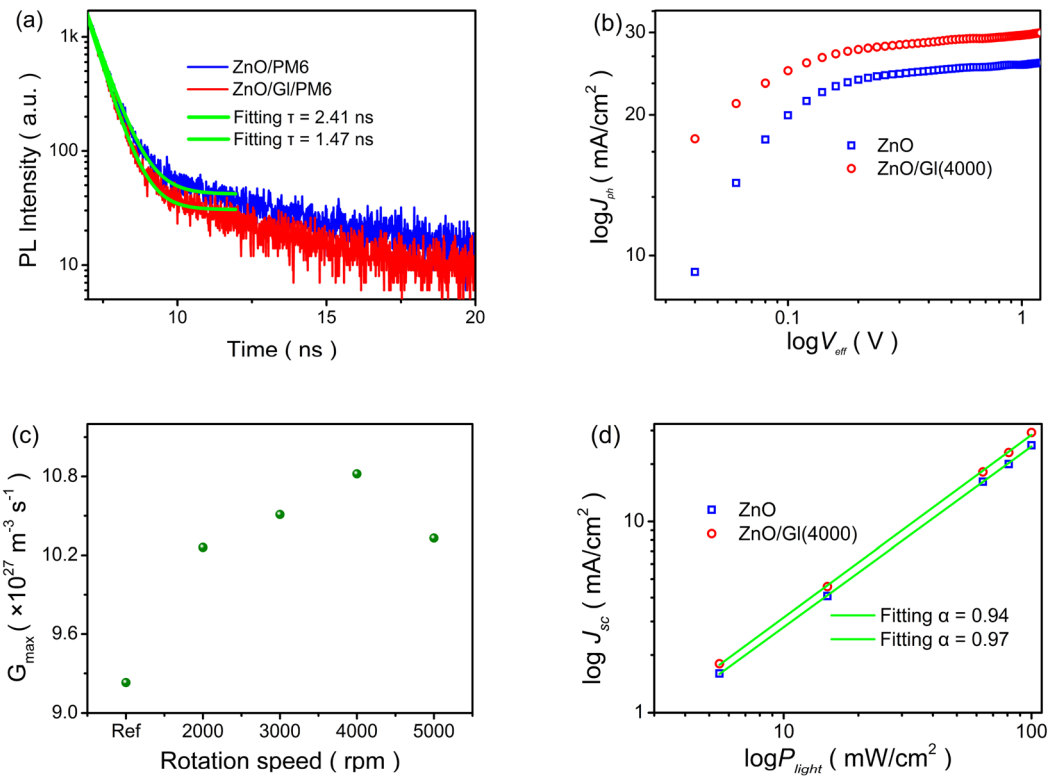

Fig. 6 (a) TRPL spectra of ZnO/PM6 and ZnO/Gl(4000)/PM6, (b) plots of log J_{ph} *versus* log V_{eff} for OSCs based on ZnO and ZnO/Gl(4000) ETLs, (c) G_{max} obtained from the reference cell and cells with ZnO/Gl(X) ETLs, and (d) plots of log J_{sc} *versus* log P_{light} of OSCs.

 This journal is © The Royal Society of Chemistry 2023

Open Access Article. Published on 19 December 2022. Downloaded on 2/7/2026 11:24:43 AM.
This article is licensed under a Creative Commons Attribution 3.0 Unported Licence.

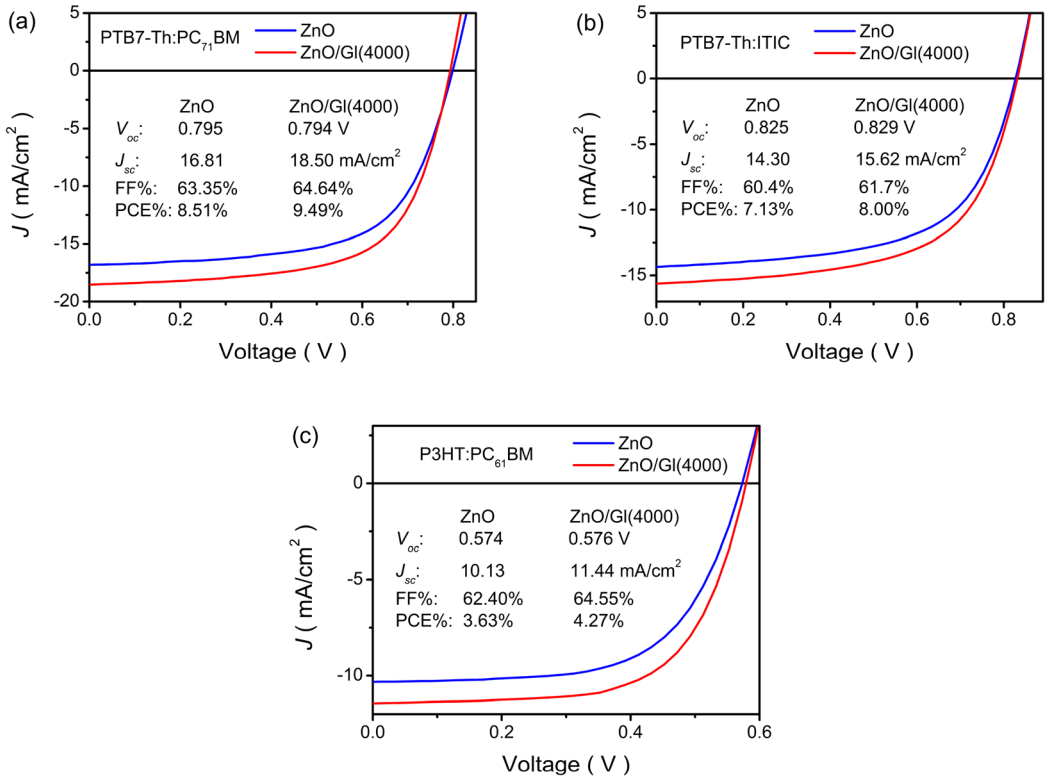

Fig. 7 J–V curves of cells based on different light absorbers using ZnO and ZnO/Gl(4000) as ETLs: (a) PTB7-Th:$PC_{71}BM$ light absorber, (b) PTB7-Th:ITIC light absorber, and (c) P3HT:$PC_{61}BM$ light absorber.

efficient light photon absorption in cells using ZnO/Gl(X) as ETLs, which could contribute to improved J_{sc} in these cells.

The dependence of J_{sc} on incident light intensity (P_{light}) was investigated to reveal charge recombination behaviors in cells with different ETLs.[34] Fig. 6d and S7† display the plots of the log J_{sc} *versus* log P_{light} of cells with ZnO and ZnO/Gl(4000) ETLs. The power law exponent of α was obtained by linear fitting and α values of 0.94 and 0.97 were extracted from the reference cell with the ZnO ETL and the cell with the ZnO/Gl(4000) ETL, respectively. The increased α (close to 1) in the ZnO/Gl(4000) ETL-based cell indicated less bimolecular recombination loss,[35] which helped to realize improved J_{sc}, FF and PCE in ZnO/Gl(X) ETL-based cells.

The ZnO/Gl(X) ETLs were also applied in blends of PTB7-Th:$PC_{71}BM$, PTB7-Th:ITIC, and P3HT:$PC_{61}BM$ light absorber-based OSCs. Impressive enhancements were observed in these cells after the introduction of Gl. As shown in Fig. 7 and Table S2,† >11% enhancements were obtained from these light absorber-based cells after the insertion of Gl compared to the reference cell with the ZnO ETL. These results demonstrated the general applicability of ZnO/Gl(X) as an ETL in fullerene and non-fullerene light absorber-based OSCs.

3. Conclusions

In conclusion, Gl was inserted between a ZnO ETL and light absorbers in inverted OSCs. Due to the hydrogen-bonding interaction between CO and OH groups, the insertion of Gl not only smoothened the interfacial contact, but also passivated OH caused surface defects on the ZnO film. Furthermore, the introduction of Gl improved the junction characteristics, contributed to electron extraction and transport processes, and suppressed bimolecular recombination loss in OSCs. In PM6:Y6 light absorber-based cells, a champion efficiency of 18.03% was obtained, which is >11% higher than that of the reference cell (16.15%). Impressive enhancements (>11%) were also observed in different fullerene and non-fullerene blend light absorber (PTB7-Th:$PC_{71}BM$, PTB7-Th:ITIC, and P3HT:$PC_{61}BM$)-based cells, which proved the general applicability of ZnO/Gl(X) as ETLs. A novel strategy by applying Gl on top of ZnO was demonstrated to design highly efficient ETLs for OSCs.

Author contributions

Zhongqiang Wang: experimental design, data analysis, writing, and funding acquisition. Yabing Ren, Jiawei Meng, Xuefeng Zou, and Shenjian Wang: experimental operation, data curation, and data validation. Min Zhao: data analysis and funding acquisition. Hua Wang, Yuying Hao, and Bingshe Xu: resources and project administration. Ergang Wang: data analysis, funding acquisition, manuscript review and editing. Shougen Yin: resources and supervision. All authors contributed to the final polishing of the manuscript.

Conflicts of interest

There are no conflicts to declare.

Open Access Article. Published on 19 December 2022. Downloaded on 2/7/2026 11:24:43 AM. This article is licensed under a Creative Commons Attribution 3.0 Unported Licence.

Acknowledgements

This work was supported by the Shanxi Provincial Natural Science Foundation of China (Grant No. 20210302123149 and 20210302123115) and Research Project Supported by Shanxi Scholarship Council of China (Grant No. 2022-046). This work was carried out with the support of the Open Foundation of Key Laboratory of Display Materials and Photoelectric Devices of Tianjin University of Technology. E. W. thanks the Swedish Research Council (2016-06146 and 2019-02345), the Swedish Research Council Formas, the Knut and Alice Wallenberg Foundation (2017.0186 and 2016.0059) and the Swedish Energy Agency (P2021-90067) for financial support.

References

1 Y. Li, X. Huang, K. Ding, H. K. M. Sheriff, L. Ye, H. Liu, C.-Z. Li, H. Ade and S. R. Forrest, *Nat. Commun.*, 2021, **12**, 5419.
2 C. Li, J. Zhou, J. Song, J. Xu, H. Zhang, X. Zhang, J. Guo, L. Zhu, D. Wei, G. Han, J. Min, Y. Zhang, Z. Xie, Y. Yi, H. Yan, F. Gao, F. Liu and Y. Sun, *Nat. Energy*, 2021, **6**, 605–613.
3 Y. Zhang, Y. Ji, Y. Zhang, W. Zhang, H. Bai, M. Du, H. Wu, Q. Guo and E. Zhou, *Adv. Funct. Mater.*, 2021, **32**, 2205115.
4 P. Bi, S. Zhang, Z. Chen, Y. Xu, Y. Cui, T. Zhang, J. Ren, J. Qin, L. Hong, X. Hao and J. Hou, *Joule*, 2021, **5**, 2408–2419.
5 R. Sun, Y. Wu, X. Yang, Y. Gao, Z. Chen, K. Li, J. Qiao, T. Wang, J. Guo, C. Liu, X. Hao, H. Zhu and J. Min, *Adv. Mater.*, 2022, **34**, 2110147.
6 Y. Cui, Y. Xu, H. Yao, P. Bi, L. Hong, J. Zhang, Y. Zu, T. Zhang, J. Qin, J. Ren, Z. Chen, C. He, X. Hao, Z. Wei and J. Hou, *Adv. Mater.*, 2021, **33**, 2102420.
7 L. Zhu, M. Zhang, J. Xu, C. Li, J. Yan, G. Zhou, W. Zhong, T. Hao, J. Song, X. Xue, Z. Zhou, R. Zeng, H. Zhu, C.-C. Chen, R. Mackenzie, Y. Zou, J. Nelson, Y. Zhang, Y. Sun and F. Liu, *Nat. Mater.*, 2022, **21**, 656–663.
8 C. He, Y. Pan, Y. Ouyang, Q. Shen, Y. Gao, K. Yan, J. Fang, Y. Chen, C.-Q. Ma, J. Min, C. Zhang, L. Zuo and H. Chen, *Energy Environ. Sci.*, 2022, **15**, 2537–2544.
9 K. Chong, X. Xu, H. Meng, J. Xue, L. Yu, W. Ma and Q. Peng, *Adv. Mater.*, 2022, **34**, 2109516.
10 J. Song and Z. Bo, *Sci. China Chem.*, 2019, **6**, 9–13.
11 Q. Nie, A. Tang, Q. Guo and E. Zhou, *Nano Energy*, 2021, **87**, 106174.
12 Y. Liu, J. Song and Z. Bo, *Chem. Commun.*, 2021, **57**, 302–314.
13 H. Meng, C. Liao, M. Deng, X. Xu, L. Yu and Q. Peng, *Angew. Chem., Int. Ed.*, 2021, **60**, 22554–22561.
14 X. Cai, T. Yuan, X. Liu and G. Tu, *ACS Appl. Mater. Interfaces*, 2017, **9**, 36082–36089.
15 H. Gao, X. Wei, R. Yu, F.-Y. Cao, Y. Gong, Z. Ma, Y.-J. Cheng, C.-S. Hsu and Z. Tan, *Adv. Opt. Mater.*, 2022, **10**, 2102031.
16 K. Pandi, K. Peramaiah and B. Neppolian, *ACS Appl. Energy Mater.*, 2021, **4**, 11480–11487.
17 Y. Tao, H. Liu, D. Wang, F. Zhao, Z. Chen, H. Zhu, H. Chen and C.-Z. Li, *Infomat*, 2022, **4**, e12276.
18 X. Zhou, X. Fan, X. Sun, Y. Zhang and Z. Zhu, *Nanoscale Res. Lett.*, 2015, **10**, 29.
19 C. Hou and H. Yu, *Chem. Eng. J.*, 2021, **407**, 127192.
20 J. Zheng, Y. Luo, X. Wen, Q. Zhang, Y. Song, J. Zhou, N. Jiang, L. Liu, F. Huang and Z. Xie, *J. Mater. Chem. A*, 2021, **9**, 9616–9623.
21 G. K. Poduval, L. Duan, M. A. Hossain, B. Sang, Y. Zhang, Y. Zou, A. Uddin and B. Hoex, *Sol. RRL*, 2020, **4**, 2000241.
22 X. Liu, Z. Zheng, J. Wang, Y. Wang, B. Xu, S. Zhang and J. Hou, *Adv. Mater.*, 2022, **34**, 2106453.
23 C.-Z. Li, J. Huang, H. Ju, Y. Zang, J. Zhang, J. Zhu, H. Chen and A. K.-Y. Jen, *Adv. Mater.*, 2016, **28**, 7269–7275.
24 M. Cui, D. Li, X. Du, N. Li, Q. Rong, N. Li, L. Shui, G. Zhou, X. Wang, C. J. Brabec and L. Nian, *Adv. Mater.*, 2020, **32**, 2002973.
25 N. S. Inamuddin, M. I. Ahamed, S. Kanchi and H. A. Kashmery, *Sci. Rep.*, 2020, **10**, 5052.
26 S. Zhou, X. Zheng, X. Yu, J. Wang, J. Weng, X. Li, B. Feng and M. Yin, *Chem. Mater.*, 2007, **19**, 247–253.
27 R. Zhang, M. Zhao, Z. Wang, Z. Wang, B. Zhao, Y. Miao, Y. Zhou, H. Wang, Y. Hao, G. Chen and F. Zhu, *ACS Appl. Mater. Interfaces*, 2018, **10**, 4895–4903.
28 D. Zhou, Y. Qin, R. Zhong, H. Xu, Y. Tong, B. Hu and Y. Xie, *J. Mater. Sci.: Mater. Electron.*, 2018, **29**, 18458–18464.
29 Y. Chen, C. Lin, T. Guo and T. Wen, *ACS Appl. Mater. Interfaces*, 2018, **10**, 26805–26811.
30 C. Huang and H. Yu, *ACS Appl. Mater. Interfaces*, 2020, **12**, 19643–19654.
31 A. Classen, C. L. Chochos, L. Lueer, V. G. Gregoriou, J. Wortmann, A. Osvet, K. Forberich, I. McCulloch, T. Heumueller and C. J. Brabec, *Nat. Energy*, 2020, **5**, 711–719.
32 S. Lee, Y. Kim, D. Kim, D. Jeong, G.-U. Kim, J. Kim and B. J. Kim, *Macromolecules*, 2021, **54**, 7102–7112.
33 X. Xiong, X. Xue, M. Zhang, T. Hao, Z. Han, Y. Sun, Y. Zhang, F. Liu, S. Pei and L. Zhu, *ACS Energy Lett.*, 2021, **6**, 3582–3589.
34 S. Jung, J. Lee, U. Kim and H. Park, *Sol. RRL*, 2019, **4**, 1900420.
35 J. Yu, Y. Xi, C.-C. Chueh, J.-Q. Xu, H. Zhong, F. Lin, S. B. Jo, L. D. Pozzo, W. Tang and A. K.-Y. Jen, *Nano Energy*, 2017, **39**, 454–460.

 This journal is © The Royal Society of Chemistry 2023